OPEN ACCESS

Epitaxial growth and stress relaxation of vapor-deposited Fe–Pd magnetic shape memory films

New Journal of Physics
The open-access journal for physics

Epitaxial growth and stress relaxation of vapor-deposited Fe–Pd magnetic shape memory films

L Kühnemund[1], T Edler[1,4], I Kock[1], M Seibt[2] and S G Mayr[1,3,4]

[1] I. Physikalisches Institut, Georg-August-Universität Göttingen, Friedrich-Hund-Platz 1, D-37077 Göttingen, Germany

[2] IV. Physikalisches Institut, Georg-August-Universität Göttingen, Friedrich-Hund-Platz 1, D-37077 Göttingen, Germany

[3] Leibniz-Institut für Oberflächenmodifizierung e.V., Translationszentrum für regenerative Medizin und Fakultät für Physik und Geowissenschaften, Universität Leipzig, Permoserstrasse 15, D-04318 Leipzig, Germany

E-mail: tobias.edler@physik.uni-goettingen.de and Stefan.Mayr@IOM-Leipzig.de

New Journal of Physics **11** (2009) 113054 (14pp)
Received 6 August 2009
Published 30 November 2009
Online at http://www.njp.org/
doi:10.1088/1367-2630/11/11/113054

Abstract. To achieve maximum performance in microscale magnetic shape memory actuation devices epitaxial films several hundred nanometers thick are needed. Epitaxial films were grown on hot MgO substrates (500 °C and above) by e-beam evaporation. Structural properties and stress relaxation mechanisms were investigated by high-resolution transmission electron microscopy, *in situ* substrate curvature measurements and classical molecular dynamics (MD) simulations. The high misfit stress incorporated during Vollmer–Weber growth at the beginning was relaxed by partial or perfect dislocations depending on the substrate temperature. This relaxation allowed the avoidance of a stress-induced breakdown of epitaxy and no thickness limit for epitaxy was found. For substrate temperatures of 690 °C or above, the films grew in the fcc austenite phase. Below this temperature, iron precipitates were formed. MD simulations showed how these precipitates influence the movements of partial dislocations, and can thereby explain the higher stress level observed in the experiments in the initial stage of growth for these films.

[4] Author to whom any correspondence should be addressed.

Contents

1. Introduction

The magnetic shape memory (MSM) effect is a promising candidate for realizing actuation in microsystems as well as in smart sensor concepts as required, e.g. in micro-electromechanical systems, and has attracted significant interest in recent years [1]–[6]. Even though higher strains have been reported for Ni–Mn–Ga [7], the Fe–Pd system in the proximity of the composition $Fe_{70}Pd_{30}$ [1] has several advantages for practical applications, including its high ductility and the orientation of its easy axis of magnetization along the long *c*-axis of the martensite, allowing the use of an out-of-plane magnetic field in a thin-film-actuator.

While Fe–Pd bulk properties have been studied thoroughly already [8], little is known about Fe–Pd thin films around the composition $Fe_{70}Pd_{30}$. Recently, the growth of very thin epitaxial films on MgO substrates produced by pulsed laser deposition (PLD) has been reported [9]. However, in these films epitaxy breaks down at a thickness of 10–20 nm because of massive (111)-twinning induced by strong tensile stress [10]. While Sugimura *et al* [2] and Inoue *et al* [11] reported on MSM Fe–Pd thin films grown by sputtering, little research has been conducted on thin films grown by thermal vapor deposition. The latter provides growth conditions closer to thermal equilibrium compared to sputtering and PLD, where the kinetic energies of the deposited atoms are considerably higher, and therefore have a major influence on film properties. Polycrystalline thin films have already been prepared [12], but epitaxial (i.e. single crystalline) films are necessary to achieve maximum strain and performance in applications.

For investigations of basic atomic scale processes that determine the macroscopic properties of epitaxial Fe–Pd thin films, transmission electron microscopy (TEM) investigations provide information on the atomic structure, whereas *in situ* mechanical stress measurements reveal valuable information about microscopic processes during and after film growth. In order to gain insight into the mechanisms and kinetics of the stress relaxation processes, molecular dynamics (MD) simulations based on the results of TEM investigations as well as the results of the stress measurements were run to directly observe the atomic processes.

2. Experimental details

$Fe_{70}Pd_{30}$ thin films were co-deposited by electron-beam evaporation from independently rate-controlled elemental sources in a UHV system [13] with a base pressure below 3×10^{-10} mbar.

The films discussed here were grown with a total rate of about 0.15 nm s^{-1} on highly polished MgO (100) single crystal substrates, which were heated to temperatures between 400 and 750 °C by a radiation heater from the back side. A calibration was conducted between the temperatures of an additional thermocouple attached directly to a substrate and the setpoint of the heating system. In order to ensure thermal homogeneity and to desorb a possible layer of hydroxide from the surface, the substrate temperature was kept constant for at least 90 min before deposition. For comparison, one film grown on amorphous SiO_2 at a temperature of 770 °C was also investigated.

Stress measurements were performed using a single laser beam deflection dilatometer, as described previously [14], while the rectangular substrate (dimensions 25 mm × 10 mm × 0.22 mm) was clamped to the holder with one short side. For this geometry, the average film stress $\langle\sigma\rangle$ times film thickness t_f can be calculated from the substrate curvature using the modified Stoney equation [15]:

$$\langle\sigma\rangle\, t_f = \frac{1}{6} B_s t_s^2 \frac{1}{r} \tag{1}$$

with B_s being the biaxial modulus of the substrate, taken as $B_s = 3.19 \times 10^{11}$ Pa from [16], and t_s and $1/r$ being the substrate thickness and the substrate curvature, respectively. Owing to the limited dynamics range of the lock-in-amplifier used, a neutral gray filter was inserted into the laser beam path at a film thickness 22 nm during the growth of the film prepared at 630 °C. This change in the optical setup leads to the observed deviations from a linear slope at this thickness.

Films with total thicknesses between 30 and 500 nm were studied, which is to be taken as mass equivalent thicknesses. Within the limitations of energy dispersive x-ray spectroscopy (EDX) measurements on thin films, a Pd content of about 30 at.% was confirmed with a system manufactured by the Thermo Electron Corporation attached to an LEO supra 35 scanning electron microscope that was also used for imaging. The surface morphology was confirmed with atomic force microscopy (AFM) topographs, taken with a Veeco Nanoscope IV system in tapping mode, which are not shown here. The crystal structure of the films was characterized by x-ray θ–2θ scans performed with a Bruker AXS D8 advance ™x-ray diffractometer and Cu K_α radiation as well as by texture measurements on the [113]-pole with a Philips X'pert system and Co K_α radiation to prove epitaxy. Thin lamellae were cut from the samples with an FEI Nova Nanolab 200 focused ion beam (FIB) system using Ga^+ ions after application of a Pt protection layer, and then studied in a Philips CM200-UT-FEG TEM operated at 200 kV.

3. Experimental results

The three films that will be discussed in more detail here were prepared at different substrate temperatures, while all other growth parameters (esp. the evaporation rates) were kept constant in order to ensure the comparability of these samples. Characterizations with respect to basic growth mode show a Volmer–Weber growth for all films investigated. A continuous film is formed at a critical thickness, which increases with increasing substrate temperature. For a substrate temperature of 630 °C SEM images (see figure 1) and AFM topographs confirm that the islands have coalesced at about 50 nm thickness, while for films grown at a substrate temperature of 690 °C the films are not completely closed at a thickness of 100 nm.

The phases, structures and lattice parameters of the films were investigated for different deposition temperatures, summarized in table 1. For films grown at 690 °C or above TEM diffraction patterns confirm the phase to be the fcc austenite with a cube-on-cube relationship

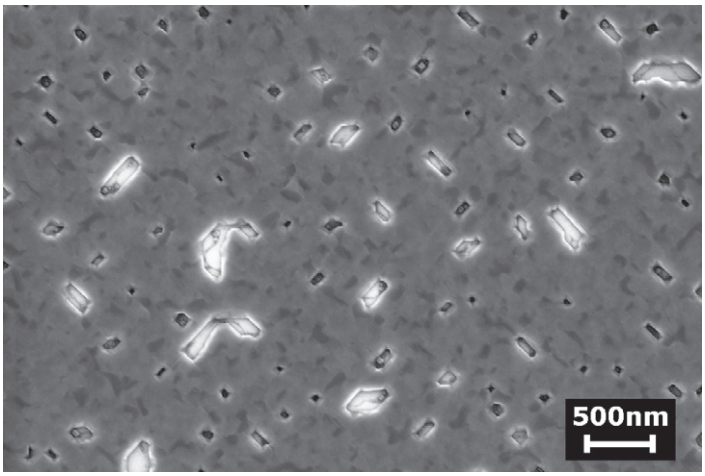

Figure 1. SEM image of a film grown at 630 °C, film thickness 45 nm. The islands have almost completely coalesced to a smooth, closed film. The remaining holes (shown either as dark or bright rectangles, depending on whether they reach down to the substrate or not) and the terraces show a rectangular shape, with a preferred orientation along the substrate (100) direction.

Table 1. Film properties for different substrate temperatures. Films deposited at 630 °C and below show partial demixing and microtwins, whereas films deposited at 690 °C and above consist of the fcc austenite only. Epitaxial growth is observed for all films grown at 500 °C and above.

Deposition temperature	500 °C	600 °C	630 °C	690 °C
Phase(s)	$Fe_{70}Pd_{30}$ fcc $Fe_{50}Pd_{50}$ $L1_0$ Fe bcc	$Fe_{70}Pd_{30}$ fcc $Fe_{50}Pd_{50}$ $L1_0$ Fe bcc	$Fe_{70}Pd_{30}$ fcc $Fe_{50}Pd_{50}$ $L1_0$ Fe bcc	$Fe_{70}Pd_{30}$ fcc
Microtwins	Yes	Yes	Yes	No
Epitaxy	Yes	Yes	Yes	Yes

between film and substrate, as was also observed in the initial stage of films prepared by PLD [9]. The lattice parameter as calculated from the TEM diffraction patterns as well as the (200) peak in the x-ray diffraction (XRD) spectra is $a = 3.76 \times 10^{-10}$ m, being consistent with the results obtained by Cui *et al* [8] for bulk $Fe_{70}Pd_{30}$. Growth at temperatures below 690 °C leads to partial demixing of the films. In addition to the $Fe_{70}Pd_{30}$ fcc peak mentioned above, the XRD-spectra of these films show a bcc Fe (200) peak (lattice parameter $a = 2.87 \times 10^{-10}$ m) as well as a (200) and an additional superstructure peak from the ordered $Fe_{50}Pd_{50}$ $L1_0$ phase leading to an out-of-plane lattice parameter of $c = 3.67 \times 10^{-10}$ m.

The microstructure of the Fe–Pd films was investigated by high-resolution TEM (HRTEM). Epitaxial growth was observed for all films grown at substrate temperatures of 500 °C and above (i.e. all films mentioned here); see the HRTEM image in figure 2. It needs to be pointed out that no thickness limit was found for epitaxial growth, either by HRTEM for film thicknesses up to 100 nm, or by texture measurements on the {113}-pole for film thicknesses up to 500 nm, the latter showing the expected fourfold symmetry with no additional peaks.

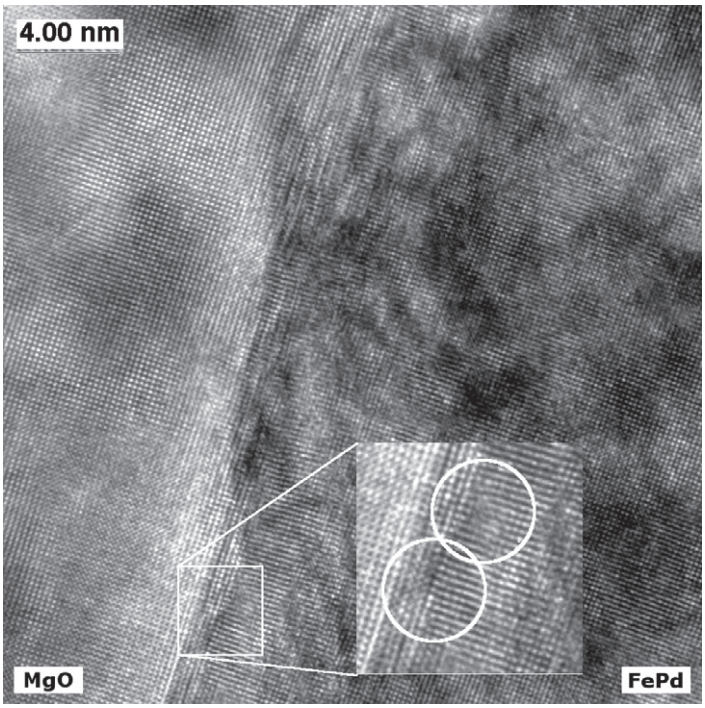

Figure 2. HRTEM image showing a [010] projection of a Fe–Pd film (thickness is 85 nm) deposited at 500 °C, showing epitaxial growth. The inset shows a magnified region of the interface region, where two edge dislocations are marked.

Careful inspection of the images shows that if Fe precipitates are present they are favorably placed flat on the substrate with a thickness range of 5–10 nm from the substrate, but there are also some Fe precipitates throughout the whole volume of the film. Dislocations could be found at the substrate–film interface for both films with and without Fe precipitates.

Microtwins are observed in all investigated lamellae of films grown at or below 630 °C, whether they are continuous or not; see figures 3 and 4. The angle of 55° between the twinning planes and the film surface in the projection onto the [110] plane of the TEM lamella is as expected for {111} twinning planes. Microtwins were not found in a non-demixing film deposited at 690 °C.

Epitaxial growth as it is observed for our films is only possible if the initial lattice misfit is reduced by relaxation. To gain further insights into the processes that occur during film growth, *in situ* substrate curvature measurements were performed during film growth. Such *in situ* mechanical stress measurements for films grown at 630 °C, 690 °C and 750 °C, respectively, are shown in figure 5. A positive slope of $\langle\sigma\rangle t_f$ corresponds to tensile stress by convention. For all films, no data points could be recorded while the substrate shutter was closed (prior to deposition while the evaporators were heated, and immediately after deposition, until the sources had cooled down). A characteristic change in substrate curvature immediately after opening the substrate shutter and during the first 120 s occurs, regardless whether a film is deposited on the substrate or not. This change in substrate curvature is a temperature effect of the deposition system. Opening of the shutter in front of the substrate at the beginning of the deposition run leads to a short drop in temperature and thus a tilting of

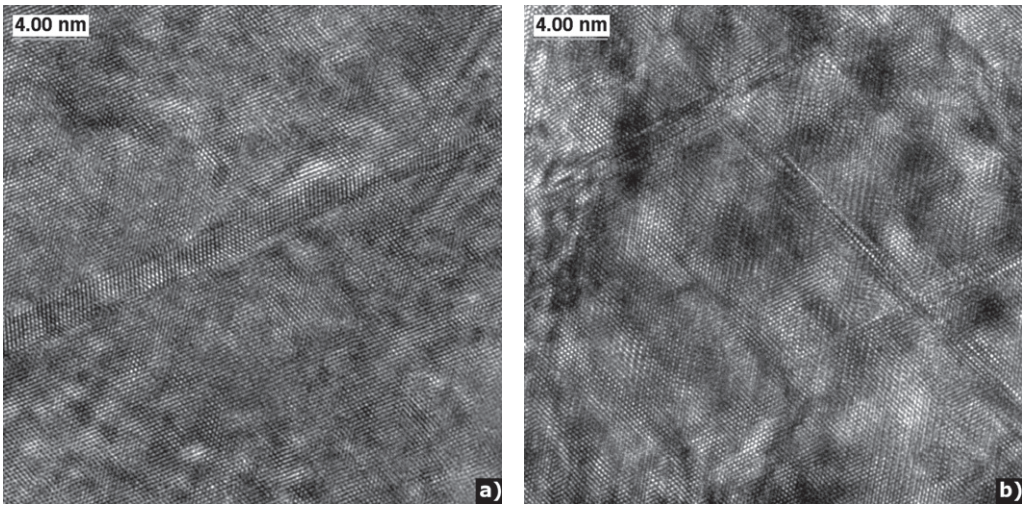

Figure 3. HRTEM images showing [011] projections of films deposited at 600 °C (a) and 500 °C (b) with film thicknesses of 70 nm and 85 nm, respectively. Microtwins are seen edge-on.

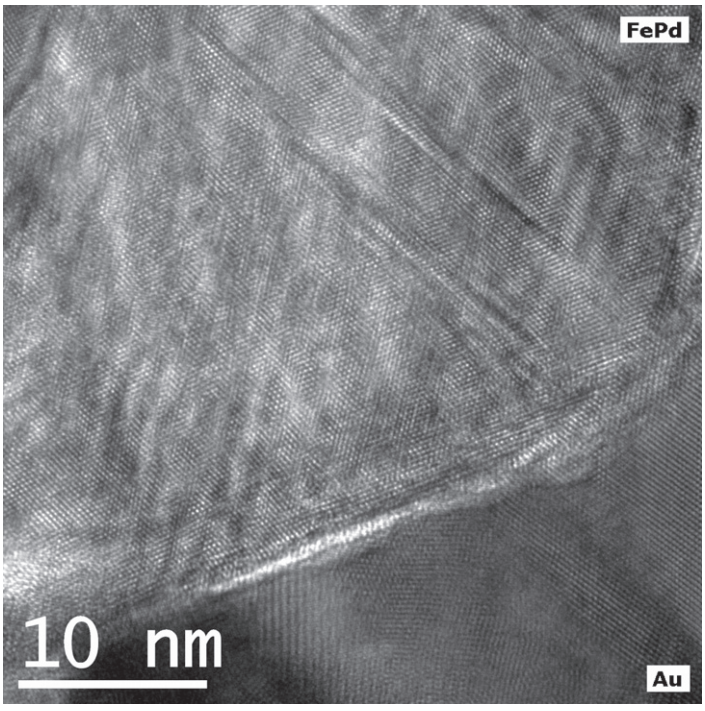

Figure 4. HRTEM image of a film deposited at 630 °C with a film thickness of 30 nm. This lamella was cut from the sample parallel to a {110} plane, showing an Fe–Pd island with two microtwins.

the substrate. Temperature measurements with a thermocouple attached to the substrate show that after about 2 min (corresponding roughly to the deposition of 15 nm) thermal equilibrium is reached again. Therefore, all data from these periods has been excluded from all graphs and evaluations.

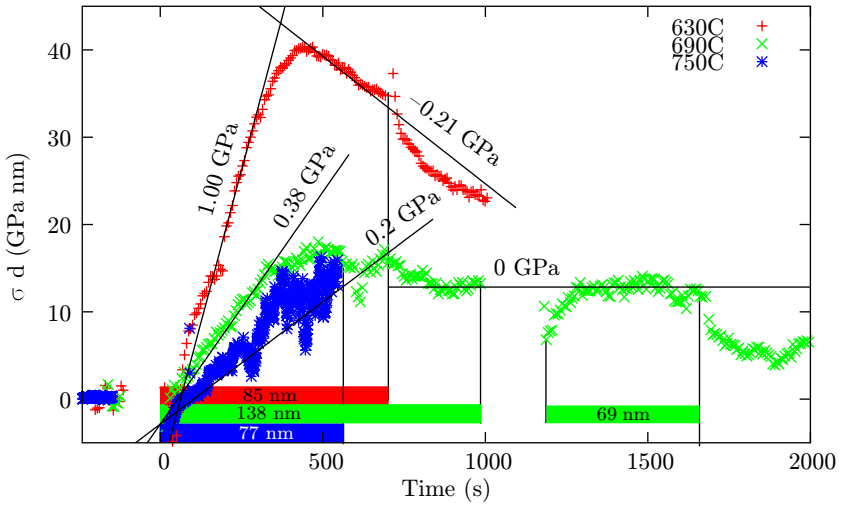

Figure 5. *In situ* substrate curvature measurement during and after film growth. Deposition periods and thickness of film are both marked with a bar in the corresponding color. In both cases, tensile stress is developed in the early stages of film growth. In the later stage, the film grown at 700 °C shows almost stress-free growth, while the film grown at 630 °C shows a decrease in substrate curvature, and a much higher overall stress. The smallest stress is observed at the highest substrate temperature of 750 °C, where the signal-to-noise-ratio (SNR) is dramatically decreased.

For the film grown at 630 °C, we observe a tensile stress of 1.00(15) GPa up to a film thickness of 50 nm, where the substrate curvature has a maximum. After this thickness, the slope is negative (−0.21(15) GPa), which corresponds either to compressive stress in the newly grown layers, or to a relaxation of the tensile stress in the deeper layers of the film. After deposition, the film stress decreases approximately exponentially as a function of time. The film prepared at 690 °C was grown in two steps. In the first step, a film with a thickness of 138 nm was deposited. Then, a shutter underneath the substrate was closed, as the material in the evaporators had to be remelted in order to ensure stable rates and evaporation characteristics over the long deposition run. Subsequently, another 69 nm were deposited on top of the film. For this film, a tensile stress of 0.38(5) GPa is observed during the first 40 nm of film growth. A maximal curvature of the substrate is reached at a thickness of 60 nm. However, this maximum is not as pronounced as for the film grown at 630 °C. The second deposition run shows a rise in curvature for the first 20 nm deposited, after which the curvature of the substrate is constant and almost identical to the level before the interruption, so the newly grown layers of the film are not stressed. After the end of the deposition, a decrease in curvature can be observed, which is of a very similar magnitude and duration as at the beginning of the second deposition run.

The film grown at 750 °C shows a dramatically decreased SNR, because the light emitted from the radiation heater is much more intense at this temperature. Nevertheless, an initial slope of about 0.2 GPa can be determined, which seems to decrease towards the end of the film growth.

4. Simulation details

The lattice constant of bcc–Fe is between the values for MgO and $Fe_{70}Pd_{30}$, so for the demixing film one could expect an iron buffer layer between the substrate and the film, and a relatively low

stress in the film. However, this film reaches the highest substrate curvature, much higher than with the non-demixing films. Precipitates not only form at the substrate–film interface, but also in the whole film volume. In order to understand the influence of these precipitates on stress relaxation, classical MD simulations were performed using a group-maintained code also used in [17]. For these simulations, FePt was chosen as a model system because of the availability of the well tested analytic bond-order potential derived in [18]. This choice can be justified by the great chemical and structural similarities between Pt and Pd, and especially the phase diagrams for Fe–Pd and Fe–Pt in the region of the 50 : 50 composition. This potential reproduces the overall properties of equiatomic alloys well, even though it is known to overestimate the twinning energy [18], so only qualitative conclusions can be drawn from the simulations. Upon straining, the simulations show a stress relaxation via microtwins, which has also been found in ordered $L1_0$ FePd-films experimentally [19].

For reference, a rectangular simulation cell of 2.5×10^5 Fe atoms and 2.5×10^5 Pt atoms was prepared in the $L1_0$ structure. In accordance with the experiments, this cell with periodic boundary conditions in all spatial directions was heated to a temperature of 900 K using a Berendsen thermostat and barostat [20] set to zero hydrostatic pressure. After a relaxation of 200 ps, the volume was kept constant, and the periodic boundary conditions were released in the z-direction. In addition to that, the last two atomic layers in the negative z-direction were fixed in order to mimic a rigid substrate, while in the positive z-direction a free surface was formed. This now resembled an infinite film in the xy-plane stuck epitaxially to a rigid substrate. The reference cell was relaxed in this geometry for an additional 40 ps. During this relaxation time, the total energy of the system reached a constant value.

Based on the results of TEM and XRD investigations, which show that the film grown at 630 °C has at least partially demixed into a $L1_0$ $Fe_{50}Pd_{50}$ matrix and bcc iron precipitates, a second cell is created from the reference cell by cutting out 10 spherical holes at random positions and placing a bcc–Fe precipitate in each. As with the reference cell, the cell with precipitates is relaxed, but for 100 ps to ensure a full relaxation of the cell. After these preparation steps, both cells are being strained with a rate of 10^{-7} per fs by rescaling the x- and y-axes. In addition, tests with other straining rates are performed, and no dependence on the strain rate is observed. During this straining process, each snapshot corresponds to a film grown on a substrate with a lattice mismatch equivalent to the applied strain.

Snapshot images for all atomic positions are taken regularly, and the central-symmetry parameter c as defined in [21] for each atom is being calculated at each snapshot. For visualization, all atoms within a certain range of this parameter are rendered using the software AtomEye [22]. This parameter quantifies how much the surrounding of a given atom deviates from a point symmetric geometry. These deviations are either caused by thermal fluctuations, or by changes in the crystal structure. For a twin boundary, which can be seen as an intrinsic stacking fault in the fcc-crystal, a value of $c = 0.042$ can be expected, whereas thermal fluctuations are significantly smaller [22], so a range of $0.014 < c < 0.4$ is chosen for all images.

5. Simulation results

The simulation cells, both with and without the iron precipitates, show a similar qualitative stress–strain behavior as shown in figure 6. Quantitatively, however, the elastic modulus and the critical strain required to trigger a stress relaxation differ. While the elastic modulus for

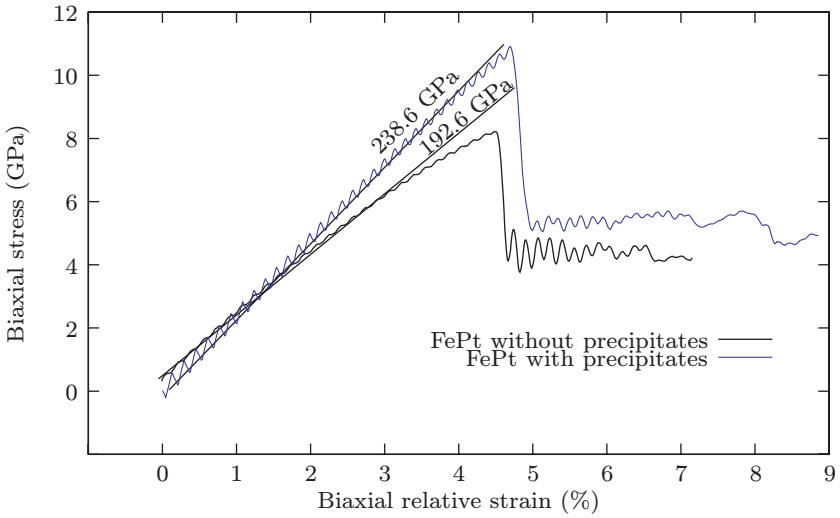

Figure 6. Stress–strain-curves obtained from MD simulations. The simulation cell with precipitates shows both a higher elastic modulus as well as a higher critical strain.

the film without precipitates is 192.6 ± 0.5 GPa (see [18] and the discussion of elastic moduli therein), the film with precipitates shows a significantly higher modulus with 238.6 ± 0.4 GPa. After reaching a critical strain of 4.5%, the film without precipitates starts to deform plastically via partial dislocations, while the cell with precipitates does so after a strain of 4.7%.

In the simulation cell without precipitates in figure 7, partial dislocations nucleate after reaching the critical stress and move through the whole cell on {111}-planes. As the strain is increased further, additional partial dislocations move through the planes adjacent to the planes of the first stacking faults, thus increasing the width of the microtwin as shown in figure 7(d). This is in excellent agreement with the experimental results on $L1_0$ FePd films [19].

In the simulation cell with precipitates, pinning of a partial dislocation at a precipitate can be observed (figure 7(a)). Shortly after, a new microtwin parallel to the blocked one intersecting the precipitate appears and moves through the sample (figure 7(b)). This new microtwin increases its thickness by the gliding of additional partial dislocations on the twin boundary planes while the blocked twin starts to disappear (figure 7(c)). This shows that the creation of a new microtwin at the cost of the energy of two stacking faults is more energetically favorable than the movement of the twin boundary through the precipitate. A direct comparison between the simulation cells for a given strain shows that the cell without precipitates has fewer but wider twins, whereas the cell with precipitates has more but thinner microtwins.

6. Discussion

In thin epitaxial $Fe_{70}Pd_{30}$ films, a temperature of 690 °C is sufficient to avoid demixing, which is significantly lower than the 760 °C which is necessary to avoid demixing in bulk samples [23]. While bulk samples are entirely governed by volume properties, surface properties have a major influence on thin films. Often, a structure stabilized at the interface is also kept stable in the volume when the old surface layer has been overgrown. Comparisons to polycrystalline films grown on amorphous SiO_2 show that the fcc structure of $Fe_{70}Pd_{30}$ is stabilized by the epitaxial

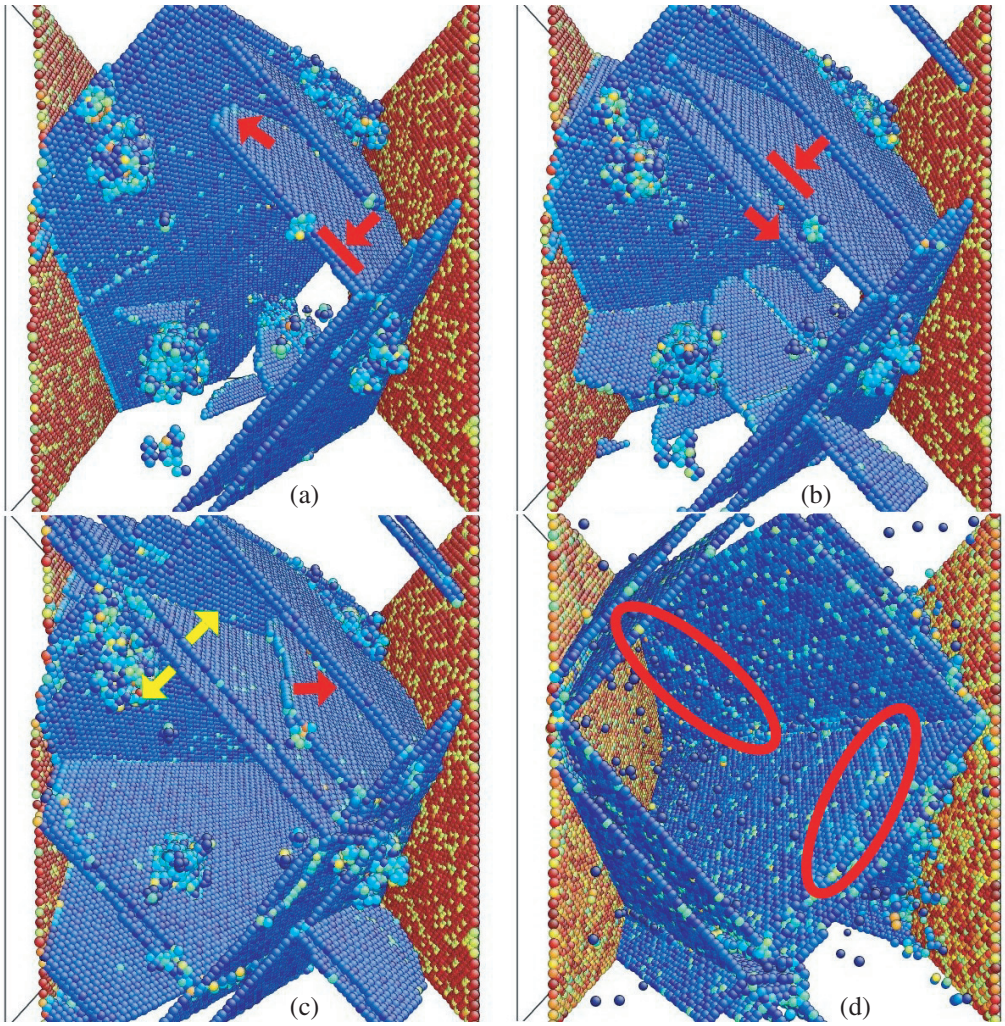

Figure 7. Movement of the stacking faults. Only atoms with a central symmetry parameter between 0.014 and 0.4 are rendered. (a)–(c) show the cell with precipitates; red arrows indicate a movement within the plane of the stacking fault, yellow arrows indicate a movement perpendicular to the plane. (d) shows new partial dislocations gliding on the edges of a microtwin in the cell without precipitates. In all pictures, the free surface is on the left-hand side, while the rigid substrate is on the right-hand side.

relation to the substrate, as these films on SiO_2 show a complete demixing at temperatures as high as 770 °C, which is even slightly above the bulk value.

In contrast to thin films grown by PLD, thermal evaporation of Fe–Pd shows no breakdown of epitaxy for thicknesses up to 500 nm. The kinetic energies of the incident atoms seem to be a key factor as they are much lower for thermal evaporation than for PLD, where generation of numerous interstitial atoms by shot-peening leads to the breakdown of epitaxy at about 10–20 nm of film thickness [10].

We attribute the strong tensile stresses observed in all films at thicknesses of 10–50 nm to the large misfit of the Fe–Pd-on-MgO growth system. A rough estimation of the misfit stress σ yields

$$\sigma = \epsilon \cdot \frac{E}{1-\nu} \approx 20\,\mathrm{GPa} \tag{2}$$

with the strain $\epsilon = 0.105$ corresponding to the substrate–film mismatch, $E = 120\,\mathrm{GPa}$ (taken from [24]) being Young's modulus of $Fe_{70}Pd_{30}$ at about 600 °C and $\nu = 1/3$ being the Poisson ratio. This value is not observed in the experiment due to incomplete coverage of the substrate, and very likely due to compensation for a part of the strain by dislocations at the film–substrate interface.

Above a thickness of about 100 nm, the film grown at 690 °C shows an almost constant curvature (apart from a stage at the beginning of the second deposition run, which then leads to the same value as before the growth interruption). As the stress in the just-grown layer is the first derivative of the substrate curvature, further atomic layers grow stress free and epitaxial growth can be maintained to very high film thicknesses despite the large initial lattice mismatch of about 10%. Together with the fact that no microtwins were observed in the samples prepared above 690 °C, this suggests that during film growth edge dislocations are intrinsically incorporated into the film, until the misfit is compensated for and the equilibrium lattice constant of the $Fe_{70}Pd_{30}$ film is reached at a film thickness of about 60 nm.

For the demixing films, it is favorable to create Fe precipitates between the substrate and the film, thus acting as a buffer between film and substrate as the misfit for 45° rotated growth of α-Fe is only about 3.4%. Stress relaxation via partial dislocation motion has been observed for ordered $Fe_{50}Pd_{50}$ before [25], and is also supported by our HRTEM investigation of the films grown below 690 °C. In fcc crystals, the favored glide system is $\{111\}\,\langle 110\rangle$; see e.g. [26]. As these $1/2\langle 110\rangle$ perfect dislocations can split into $1/6\langle 112\rangle$ Shockley partial dislocations, there are two kinds of mechanism expected to relax misfit strains in fcc metallic thin films. A pile-up of partial dislocations leads to the formation of microtwins [25]. An estimation of the energy cost of these two mechanisms in ordered and disordered $Fe_{50}Pd_{50}$ was carried out by Halley *et al* [19] and can easily be generalized to a broader composition range. The propagation of a perfect dislocation in a perfectly ordered $Fe_{50}Pd_{50}$ $L1_0$ structure leaves an antiphase boundary (APB) in the $\{111\}$ glide plane with an energy estimated to be $\gamma_{111}^{\mathrm{APB}} \approx 0.2\,\mathrm{J\,m^{-2}}$ [19]. This contribution vanishes in the same degree as the ordering vanishes. On the other hand, the propagation of a partial dislocation always leaves a stacking fault in the glide plane that is linked to a stacking fault energy, while the total energy of the partial dislocation is independent of chemical order. We can thus estimate the energy of the partial dislocation from the stacking fault energies of pure iron [27] and pure palladium [28] by stoichiometric average, yielding $\gamma_{111}^{\mathrm{partial}} \approx 0.17\,\mathrm{J\,m^{-2}}$ for $Fe_{70}Pd_{30}$. It stays similar for slight deviation of composition. What Halley *et al* showed for $Fe_{50}Pd_{50}$ can be generalized to $Fe_{70}Pd_{30}$: for the ordered $L1_0$ structure partial dislocations and thus microtwins are the favored mechanism for mechanical stress relaxation, whereas for a decreasing degree of order perfect dislocations become favorable.

This explains why microtwins occur in all films except for the non-demixing ones grown at high temperatures, which do not exhibit the ordered $L1_0$ phase. One can instead observe edge dislocations at the film–substrate interface in regular intervals. From the MD Simulations, it can be seen that the bcc–Fe precipitates have a negative effect on the stress relaxation via twinning: as seen in figure 7, a twin boundary can be stopped at a precipitate, and a new twin boundary

that does not intersect the precipitate is formed. From these results, it can be understood that the film with precipitates shows the highest average stress in the experiments.

For a growth temperature of 630 °C microtwins are already observed in a thin film of 30 nm thickness, which is consistent with the results obtained by Liu *et al* [29], who calculated the critical thickness for misfit twinning during growth with a tensile mismatch strain of 0.10 to be about 0.8 nm. Nevertheless, the overall trend of the stress measurement suggests that the vast majority of the stress relaxation happens at a film thickness of 50 nm, which also coincides with the thickness at which the islands coalesce to a continuous film. Before the stress is fully relaxed, it is energetically unfavorable to increase the tensile stress in the film even further by island zipping, whereas once the lattice misfit has fully been compensated the tendency to reduce the film surface leads to the formation of a continuous, smooth film. This picture is supported by the fact that the intensity of the reflected laser beam reaches a maximum shortly after the curvature has reached its maximal value. Here, the derivative of the substrate curvature, and thus the stress in the newly grown layers, is zero. The intensity of the reflected laser beam is related to the surface roughness of the film [30], so this maximum intensity is the signature of a minimum in roughness.

However, there has to be a further mechanism that can account for the exponential decay of the stress after deposition. As pure surface effects like a surface reconstruction after the end of film growth only affect the stress state in a few monolayers, this pronounced relaxation can only be volume effects. One explanation could be a dynamic balance between defects being incorporated into the film, and such defects annealing out. After the deposition has stopped these defects still heal out, while no new defects are created. This leads to the relaxation observed after the end of deposition, and could also explain the feature observed at the beginning of the second deposition run of the sample prepared at 690 °C, which shows the same inverse behavior as after the deposition, with a very similar magnitude and time constant. A massive surface roughening like an Asaro–Tiller–Grinfeld instability [31] can be excluded from the intensity of the reflected laser beam. Such a mechanism would lead to a characteristic decrease in intensity caused by surface roughening after the end of deposition and a corresponding increase when the grown is continued, which is not observed.

7. Conclusion

Despite the large lattice mismatch of roughly 10%, epitaxial growth of thick single-crystalline $Fe_{70}Pd_{30}$ films on MgO is possible by e-beam evaporation at suitable substrate temperatures. During early stages of film growth, a strong tensile stress caused by the misfit to the substrate is incorporated into the film. This stress is relaxed by different mechanisms that depend on the phase and microstructure, which are strongly influenced by the substrate temperature. For lower temperatures, a demixing into (partially $L1_0$ ordered) $Fe_{50}Pd_{50}$ and bcc–Fe precipitates is observed as expected from the bulk phase diagram. Even though coherent bcc–Fe precipitates can act as a buffer layer at the substrate–film interface, MD simulations show that the presence of such precipitates in the film volume hinders twin boundary motion, and thus leads to a higher residual stress in the film, as also observed in the experiments.

On MgO substrates, no demixing during film growth was found for substrate temperatures of 690 °C and above. The crystal structure forced upon the film by the epitaxial relation to the substrate obviously stabilizes the fcc $Fe_{70}Pd_{30}$ phase to lower temperatures than in bulk samples or in films on amorphous substrates. At the same time, bcc iron precipitates that mainly

occur at small thicknesses can act as a buffer layer, and thereby reduce the misfit dramatically, thus further stabilizing the system against demixing in later stages of film growth. These films with precipitates relax the stress via a pile-up of partial dislocations, leading to the formation of microtwins. As also observed in the MD simulations, the Fe precipitates hinder this stress relaxation and lead to a higher number of smaller twins, instead of fewer but larger twins as for pure $Fe_{50}Pd_{50}$.

Films without Fe precipitates do not show microtwins, so the stress is most likely relaxed by the introduction of perfect misfit dislocations during epitaxial growth. Once the lattice mismatch has been compensated, the epitaxy is preserved even for very high thicknesses.

Acknowledgments

We would like to thank C Mahn for technical support and V Radisch for FIB sample preparation. This project is funded by the German DFG SPP 1239, TP C4.

References

[1] James R D and Wuttig M 1998 Magnetostriction of martensite *Phil. Mag.* A **77** 1273–99

[2] Sugimura Y, Cohen-Karni T, McCluskey P and Vlassak J 2003 Fabrication and characterization of Fe–Pd ferromagnetic shape-memory thin films *Materials and Devices for Smart Systems (Mater. Res. Soc. Symp. Proc.)* vol 785 ed Y Furuya, E Quandt, Q Zhang, K Inoue and M Shahinpoor (Pittsburgh, PA: Material Research Society)

[3] Buschbeck J, Schultz L and Fähler S 2008 Epitaxial Fe–Pd magnetic shape memory films-issues for preparation and applications *Proc. Actuator 2008, 11th Int. Conf. on New Actuators* (Bremen: Germany) p 750

[4] Suorsa I, Tellinen J, Ullakko K and Pagounis E 2004 Voltage generation induced by mechanical straining in magnetic shape memory materials *J. Appl. Phys.* **95** 8054

[5] Thienhaus S, Zamponi C, Rumpf H, Hattrick-Simpers J, Takeuchi I and Ludwig A 1999 High-throughput characterization of shape memory thin films using automated temperature-dependent resistance measurements *Materials Research Society Symposium Proc.* vol 894 (Warrendale, PA: Materials Research Society) p 197

[6] Söderberg O, Sozinov A and Lindroos V K 2006 *Handbook of Magnetic Materials* vol 16 ed K H J Buschow (Amsterdam: Elsevier) Chapter 1 pp 1–39

[7] Sozinov A, Likhachev A A, Lanska N and Ullakko K 2002 Giant magnetic-field-induced strain in NiMnGa seven-layered martensitic phase *Appl. Phys. Lett.* **80** 1746

[8] Cui J, Shield T W and James R D 2004 Phase transformation and magnetic anisotropy of an iron-palladium ferromagnetic shape-memory alloy *Acta Mater.* **52** 35–47

[9] Buschbeck J, Lindemann I, Schultz L and Fähler S 2007 Growth, structure and texture of epitaxial $Fe_{100-x}Pd_x$ films deposited on MgO (100) at room temperature: an x-ray diffraction study *Phys. Rev.* B **76** 205421

[10] Edler T, Buschbeck J, Mickel C, Fähler S and Mayr S G 2008 Mechanisms of stress generation and relaxation during pulsed laser deposition of epitaxial fe–pd magnetic shape memory alloy films on MgO *New J. Phys.* **10** 063007

[11] Inoue S, Inoue K, Koterazawa K and Mizuuchi K 2003 Shape memory behavior of Fe–Pd alloy thin films prepared by dc magnetron sputtering *Mater. Sci. Eng.* A **339** 29–34

[12] Kock I, Edler T and Mayr S G 2008 Growth behavior and intrinsic properties of vapor-deposited iron palladium thin films *J. Appl. Phys.* **103** 046108

[13] Mayr S G, Moske M and Samwer K 1999 Identification of key parameters by comparing experimental and simulated growth of vapor-deposited amorphous Zr-Al-Cu films *Phys. Rev.* B **60** 16950

[14] Mayr S G and Samwer K 2001 Model for intrinsic stress formation in amorphous thin films *Phys. Rev. Lett.* **87** 36105
[15] Stoney G G 1909 The tension of metallic films deposited by electrolysis *Proc. R. Soc.* A **82** 172–5
[16] Turley J and Sines G 1971 The anisotropy of young's modulus, shear modulus and Poisson's ratio in cubic materials *J. Phys. D: Appl. Phys.* **4** 264–71
[17] Neudecker M and Mayr S G 2009 Dynamics of shear localization and stress relaxation in amorphous Cu50Ti50 *Acta Mater.* **57** 1437–1441
[18] Müller M, Erhart P and Albe K 2007 Thermodynamics of $L1_0$ ordering in FePt nanoparticles studied by Monte Carlo simulations based on an analytic bond-order potential *Phys. Rev.* B **76** 155412
[19] Halley D, Marty A, Bayle-Guillemaud P, Gilles B, Attane J P and Samson Y 2004 Chemical order and selection of the mechanism for strain relaxation in epitaxial FePd (Pt) thin layers *Phys. Rev.* B **70** 174438
[20] Berendsen H J C, Postma J P M, van Gunsteren W F, DiNola A and Haak J R 1984 Molecular dynamics with coupling to an external bath *J. Chem. Phys.* **81** 3684
[21] Kelchner C L, Plimpton S J and Hamilton J C 1998 Dislocation nucleation and defect structure during surface indentation *Phys. Rev.* B **58** 11085–8
[22] Li J 2003 AtomEye: an efficient atomistic configuration viewer *Modelling Simul. Mater. Sci. Eng.* **11** 173–7
[23] Massalski T B 1986 *Binary Alloy Phase Diagrams* (Ohio: American Society for Metals)
[24] Nakayama T, Kikuchi M and Fukamichi K 1980 Young's modulus and the δe effect of Fe-Pd invar alloys *J. Phys. F: Met. Phys.* **10** 715–9
[25] Halley D, Samson Y, Marty A, Bayle-Guillemaud P, Beigné C, Gilles B and Mazille J E 2002 Anomaly of strain relaxation in thin ordered FePd layers *Phys. Rev.* B **65** 205408
[26] Haasen P 1996 3rd ed *Physical Metallurgy* (Cambridge: Cambridge University Press)
[27] Okrainets P N and Pishak V K 1978 *Metallofiz. Noveishie Tekhnol.* **72** 31
[28] Dillamore I L and Smallman R E 1965 The stacking-fault energy of fcc metals *Phil. Mag.* **12** 191–3
[29] Liu L, Zhang Y and Zhang T Y 2007 Strain relaxation in heteroepitaxial films by misfit twinning. I. Critical thickness *J. Appl. Phys.* **101** 063501
[30] Angelsky O V, Hanson S G and Maksimyak P P 1999 *Use of Optical Correlation Techniques for Characterizing Scattering Objects and Media* (Bellingham, WA: SPIE Press)
[31] Orr B G, Kessler D, Snyder C W and Sander L 1992 A model for strain-induced roughening and coherent island growth *Europhys. Lett.* **19** 33–8